NeuroImage 258 (2022) 119339

Contents lists available at ScienceDirect

NeuroImage

journal homepage: www.elsevier.com/locate/neuroimage

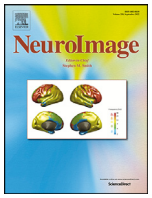

Brain intrinsic connection patterns underlying tool processing in human adults are present in neonates and not in macaques

Haojie Wen [a,b,c], Ting Xu [d], Xiaoying Wang [a,b,c], Xi Yu [a,*], Yanchao Bi [a,b,c,e,*]

[a] *State Key Laboratory of Cognitive Neuroscience*

Regarding nonhuman primates, similarities and di erences to humans have been reported on both behavioral and neural levels. The simpler forms of tool use and even tool making are not unique to humans. Animals have visual and motor experiences with objects such as gasping a stick, and some have even demonstrated simple tool use (e.g., apes and crows use sticks to forage for insects, Bentley-Condit and Smith, 2010; Fayet et al., 2020; Shumaker et al., 2011). Nevertheless, humans are arguably the only species that can make and use sophisticated tools based on causal (mechanical) understanding of the relationship between its physical properties, use and function (Johnson-Frey, 2003; Laland and Seed, 2021; Osiurak and Reynaud, 2020; Penn et al., 2008; Vaesen, 2012; Visalberghi and Limongelli, 1994), which allows them to convert ordinary objects into tools for flexible functional use as early as two years of age (Kastner et al., 2017). Neurally, in the macaque brains, object grasping or simple-tool-use is supported by a lateral network encompassing the parietal cortex, premotor area and inferior frontal gyrus (e.g., Borra et al. 2017, Obayashi et al. 2001), regions in proximity to the tool-processing areas in human adults; yet, species-di erences were observed in the left inferior parietal cortex associating with tool-use-activities (Peeters et al., 2009). The characteristics of brain connectivity pattern among these homologous brain regions, however, have not been compared across species and developmental trajectories.

Here, we empirically tested the phylogenetic and ontogenetic origins of the intrinsic tool processing network observed in human adults by comparing resting-state functional connectivity (rsFC) pattern among tool processing regions in human adults ($n = 100$) to rsFC among homologous regions in human neonates with little motor experience ($n = 118$) and in macaque monkeys with ample visual/motor experiences (adolescent and mature, $n = 25$). If the emergence of the intrinsically connected tool processing network in human adults is driven by learnt sensory-motor association based on the visual-motor/manipulation experiences with objects, then similar intrinsic connectivity pattern among the homologous regions are not predicted in human neonates, who have not developed any nonreflective motor skills and thus no object use experience, but predicted in macaques, who have extensive motor experience with objects. Alternatively, the tool network observed in human adults may be innate and (at least partly) unique to homo sapiens, supporting the human-unique complex tool making/use behaviors, and we would expect to observe similar intrinsic connectivity pattern already present among the homologous regions in the human neonate brain, and not in the macaque brain. A brain network supporting face processing (henceforth face processing network), which has been reported for both humans (Wang et al., 2016) and macaques (Schwiedrzik et al., 2015), was also assessed in these three populations as a reference point for the potential tool processing network.

2. Methods

2.1. Participants

Human adults. Resting-state images of human adults were obtained from the WU-Minn Human Connectome Project (HCP) carried out at Washington University in St. Louis (Van Essen et al., 2013, https://www.humanconnectome.org/study/hcp-young-adult). For the current study, 100 individuals (55 females, 28.3 ± 3.4 years old), coming from di erent families (i.e., not related), were randomly selected from the 1200 Subjects Data Release. The fMRI data of all selected participants met the following inclusion criteria: (1) had less than 10% of volumes with framewise displacement (FD) ≥ 0.3 mm (see details in 2.2 Image preprocessing) and (2) exhibited good coverage (>50% overlap) of the functional Regions of Interest (ROIs) selected (see details in 2.4 ROI selection and cross-population registration). This project was reviewed and approved by the Institutional Ethics Committee of Washington University in St. Louis, Missouri. All participants signed written informed consent.

Human neonates. Imaging data of human neonates were obtained from the Developing Human Connectome Project (dHCP) conducted at the Newborn Imaging Center at Evelina London Children's Hospital, London, UK (Makropoulos et al., 2018, https://www.developingconnectome.org). 118 neonates (57 females, birth age = 39.7 ± 1.9 weeks; scan age = 40.9 ± 2.1 weeks, birth weight = 3.1 ± 0.66 kg) were selected from the two data releases available at the time of data analysis for the present study based on the following inclusion criteria: (1) images were acquired within the first month (i.e., ≤ 4 weeks) after birth; (2) structural images showed no clinical concerns when evaluated by a perinatal neuroradiologist (i.e., radiology score ≤ 3); (3) ≤ 10% of scans contained excessive head movement, defined as ≥ 0.3 mm FD; (4) there was good coverage (>50% overlap) of the functional ROIs selected. Among them, 12 neonates were born pre-term (birth age range: 31.7–36.9 weeks), while the remaining 106 participants were born full-term. The dHCP was approved by the UK health Research Authority. Informed parental consent was obtained for imaging acquisition and data release.

Adolescent and adult macaques (macaca mulatta). Macaque imaging data were obtained from the PRIMatE Data Exchange (PRIME-DE)

hff6s of macaques were included in the present study. One of them was *Newcastle data*, where macaques were *awake* during image acquisition. Resting-state fMRI images were available for 10 macaques (

a100

6 5853 227.41 8 9631 6 T03 7.9701 333

Van

were scanned during natural sleep without sedation. A multiband EPI sequence was utilized with TR = 392 ms, TE = 38ms, FA = 34°, voxel size = 2.15 × 2.15 × 2.15 mm^3, MB factor = 9, and total scan time = 2300 volume (15.05 min). T2-weighted (TR = 12 s; TE = 156 ms; sensitivity encoding (SENSE) factor: axial = 2.11, sagittal = 2.58) and inversion recovery T1-weighted (TR = 4795 ms; TI = 1740 ms; TE = 8.7 ms; SENSE factor: axial = 2.26, sagittal = 2.66) multi-slice fast spin-echo images were also collected for all neonates (in-plane resolution = 0.8 × 0.8 mm^2, 1.6 mm slices overlapped by 0.8 mm, see details in Fitzgibbon et al. (2020).

Macaque monkeys (macaca mulatta). The *Newcastle data* were collected on a Vertical Bruker 4.7T primate dedicated scanner with a single channel or a 4–8 channel parallel imaging coil. All monkeys included in the current study were awake during resting-state imaging acquisition. Two resting-state sessions were collected for each monkey with 1.2 × 1.2 × 1.2 mm^3 resolution, TR = 2600 ms, TE = 17 ms, 10.8 min (250 volumes) per scan. T1-weighted images were also acquired using a modified driven equilibrium Fourier transform (MDEFT) sequence with the following parameters: TR = 750 ms, TE = 6ms, inversion delay = 700 ms, FOV = 12.8 × 9.6 cm^2 on a grid of 256 × 192 voxels, voxel size = 0.5 × 0.5 × 2 mm, number of slices = 22. Additionally, no contrast agent was used during scanning.

The *Oxford data* were collected on a 3T scanner with a 4-channel coil when macaques were under anesthesia. Again, no contrast agent was used. The acquisition parameters for the resting-state images were 2 × 2 × 2 mm^3 resolution, TR = 2s, TE =19 ms, FA = 90°, and total scan time = 53.3 min (1600 volumes). T1-weighted images for all monkeys were also acquired using a MPRAGE sequence with the following parameters: TR = 2500 ms, TE = 4.01ms, TI = 1100 ms, FA= 8°, voxel size = 0.5 × 0.5 × 0.5 mm.

2.3. Image preprocessing

Human adults. We used the HCP's minimally preprocessed resting-state data (Glasser et al., 2013), which were distortion and motion corrected and registered to MNI templates via structural images using non-linear transformations. These images were further denoised using independent component analysis (ICA) with the FMRIB's ICA-based X-noiseifier (FIX) tool (Salimi-Khorshidi et al., 2014) to e ectively identify and remove the components of spatiotemporal signals caused by non-neuronal or structural noise, including head movement (Smith et al., 2013). Moreover, volumes with ≥ 0.3 mm FD (Power et al., 2012) were identified as outlier scans with excessive motion. All human adults included in the current analyses had no more than 10% outliers (2.7% ± 0.025). Preprocessing procedures subsequently performed using the DPABI toolbox (Yan et al., 2016) included: (1) linear detrending to minimize the e ects of low-frequency drift; (2) regression of nuisance variables, including the mean white matter (WM) and the cerebrospinal fluid (CSF) signals, continuous head movement (Friston-24 parameters, i.e.,

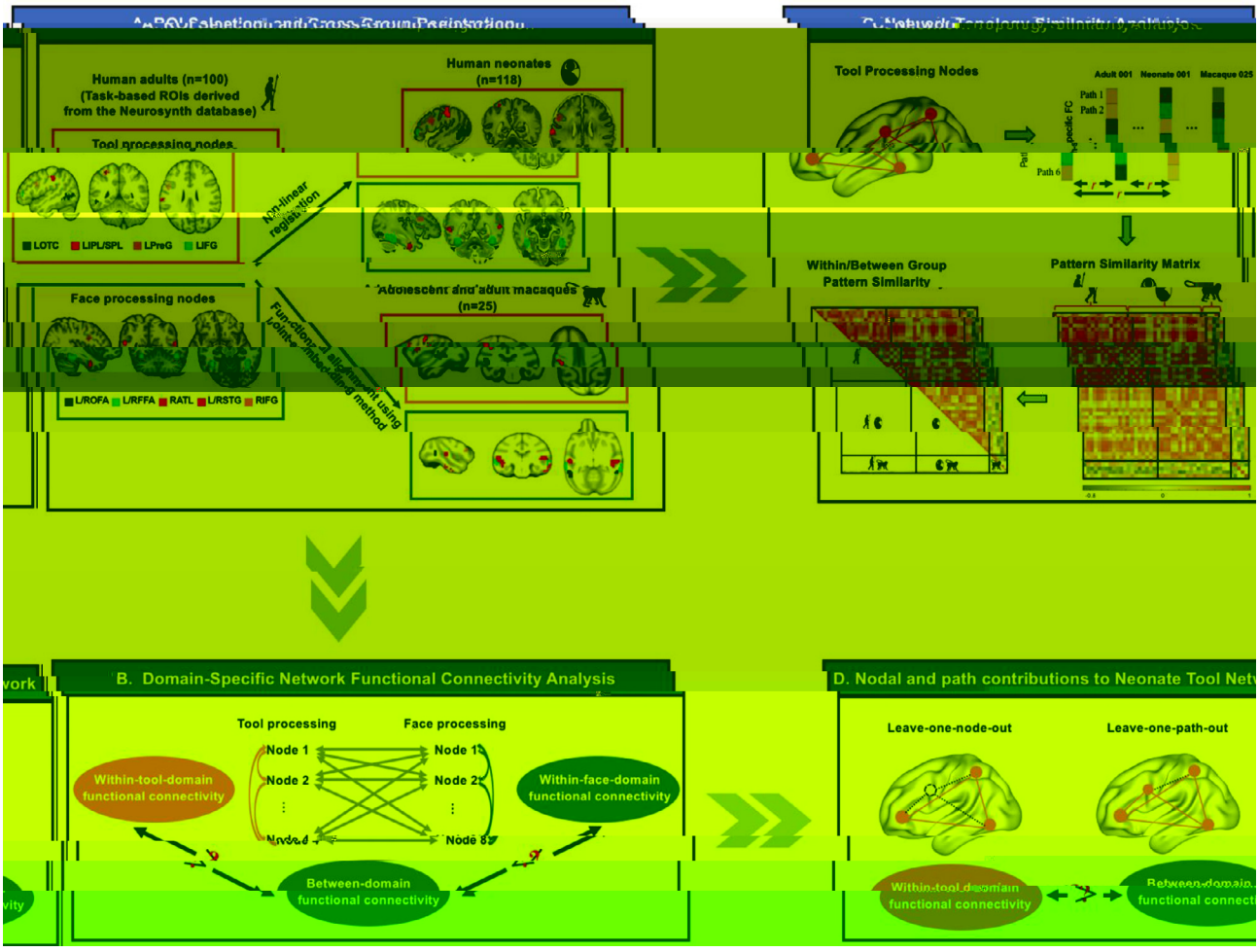

Fig. 1. Flow chart of resting-state functional connectivity (rsFC) analyses for tool and face processing networks in human adults, human neonates and macaques. A. Tool and face processing nodes are pres.00ed in slice views on standard templates for human adults (T1-weigh0ed),human neonates (T2-weigh0ed),and macaques (T1-weigh0ed).Thes. nodes were initially derived from task-based fMRI meta-analyses using the Neurosynth database and then registered to human neonate and macaque spaces using non-linear registration and functional alignment approaches, respectively. B. Intrinsic networks were first evalua0edby comparing rsFC between nodes of the same network to that of nodes belonging to di erent networks. C. A step-by-step procedure is illustrated for computing network topology similarity between groups (using the tool processing network as an example). D. Additional characterization of nodal and path contributions to the formation of the tool processing network using the leave-one-out approach. Slice views and projected brain images were prepared in Mricron (https://www.nitrc.org/projects/mricron) and BrainNet Viewer (Xia et al., 2013), respectively. LOTC: left lateral occipitotemporal cortex; LIPL/SPL: left inferior and superior parietal lobule; LPreG: left premotor gyrus; LIFG: left inferior frontal gyrus; L/ROFA: left and right occipital face areas; L/RFFA: left and right fusiform face areas; RATL: right anterior temporal lobe; L/RSTG: left and right superior temporal gyrus; RIFG: right inferior frontal gyrus.

tify functionally distinctive ROIs, resulting in right fusiform face area (RFFA), right occipital face area (ROFA) and right superior temporal gyrus (RSTG) on the right ($z = 5$ for RSTG; $z = 11$ for ROFA and RFFA) and left fusiform face area (LFFA) and left occipital face area (LOFA) on the left ($z = 8$). The stricter threshold ($z = 5$) also helped to confine the RATL to the cerebral cortex. Overall, we identified a left-hemispheric tool network and a bilateral face network (Fig. 1A, Table S2) that contained key regions commonly reported in previous meta-analyses and review papers (Lewis, 2006; Wang et al., 2020).

For neonates, these tool and face processing ROIs identified in human adults in MNI152 space were then transformed onto 40-week templates available on the dHCP- website (https://gin.g-node.org/BioMedIA/dhcp-volumetric-atlas-groupwise), using Advanced

on the preprocessed functional images of each participant using the DPABI automask function, and the overlap between such binary mask and each selected ROI was calculated, as an indication of ROI coverage. All human adults and neonates met the inclusion criteria (> 50% overlap, see 2.1 Participants), showing optimal coverage of each ROI (overlap: human adults: 96% ± 0.06, human neonates: 96% ± 0.09). Note that a lenient inclusion threshold (> 30%) was applied to the macaque groups to maximize the sample sizes, which still resulted in overall good coverage (awake: 1 excluded, remaining 95% ± 0.12; anesthetized, 3 excluded, remaining: 96% ± 0.13). Replication analyses were performed based on the data of 17 macaques using the same inclusion criterion as humans (> 50%), which did not alter the main result patterns (Fig. S3).

2.5. Resting-state functional connectivity (rsFC) analyses

For each individual from all the three groups (i.e. human adults, human neonates, and macaques), the node-based timecourse was calculated by averaging across all voxels included in each ROI. Pearson correlations were then performed on the node-based timecourse for each ROI pair and the resulting correlation coe cients were transformed to Fisher Z scores. This procedure generated an rsFC matrix for each subject. Network analyses included three major steps. First, the intrinsic tool and face processing networks were evaluated in each group by comparing the rsFC between nodes belonging to the same domain with that between nodes from di erent domains (Fig. 1B). To this aim, a one-way repeated measures ANOVA was first performed within each group to examine the potential di erences among the three sets of rsFC: the mean rsFC of the six within-tool-domain connections among the four tool processing nodes, the mean rsFC of the 28 within-face-domain connections (eight face processing nodes), the mean rsFC of the 32 between-domain connections each connecting one tool and one face processing node. Upon significant ANOVA e ects, paired *t*-tests were then carried out to evaluate the di erences between the rsFC of the within-domain connections and that of the between-domain connections for the tool and face processing networks, respectively. An intrinsic network was deemed present in a specific group if the *t*-tests revealed significantly higher within-domain than between-domain rsFC.

A set of validation analyses were subsequently performed to ensure the observed network e ects were not due to potential confounding variables of nodal distance, sample size, temporal signal-to-noise ratio (tSNR), and ROI selection methods (see Supplementary Materials 1.1 and 1.2 for details).

The second analysis focused on the network topology similarity between di erent groups. Pearson correlations were conducted on the rsFC values across paths within the tool (or face) processing network for each subject pair across all three groups (Fig. 1C), which were converted into Fisher Z scores for significance testing. One-sample *t*-tests were applied to evaluate whether each of the between-group pattern similarities were significantly greater than 0. A one-way ANOVA analysis was then performed to evaluate whether the between-group similarities di ered among the three group pairs, and post-hoc comparisons were subsequently carried out upon a significant main e ect. The *r* values for the corresponding Fisher Z scores were further reported (Fig. 3C) to more transparently present the correlation magnitudes of the network topology similarity between di erent groups.

In the final analysis, the contribution of each node and each path to the intrinsic tool network observed in human adults and neonates was investigated. A leave-one-node/path-out approach was applied, where the comparisons of within- and between- domain rsFC were re-evaluated when one node or path was removed at a time (Fig. 1D).

The Bonferroni correction for multiple comparisons was performed for all the analyses included in the current study. The Cohen's *d* and the partial $\eta 2$ e ect sizes were additionally computed for the significant *t*-test and ANOVA test results, respectively, for clearer interpretation.

3. Results

3.1. Intrinsic functional connectivity results

Human adult tool network characterization. Using the human adult resting-state dataset available in the HCP, we demonstrated that these regions being consistently activated by tools (or faces) constituted tightly connected networks, replicating previous literature (Peelen et al., 2013; Stevens et al., 2015; Wang et al., 2016). Specifically, the ANOVA analysis revealed significant group di erences ($F_{2,198} = 118.27$, $p < 0.001$, partial $\eta^2 = 0.54$) among the within-tool-domain, within-face-domain and between-domain rsFC. Post-hoc analyses further demonstrated significantly greater rsFC among the tool processing nodes and among the face processing nodes than the rsFC between tool and face processing nodes (within-tool-domain > between-domain: $t_{99} = 15.4$, $p_{corrected} < 0.001$, *Cohen's d* = 1.54; within-face-domain > between-domain: $t_{99} = 15.4$, $p_{corrected} < 0.001$, *Cohen's d* = 1.54, Fig. 2A).

Tool homologous intrinsic network structure present in human neonates. Based on the resting-state images of human neonates available from dHCP, significant di erences among the within-tool-domain, within-face-domain and between-domain rsFC were first revealed by the ANOVA analysis ($F_{2,234} = 126.3$, $p < 0.001$, partial $\eta^2 = 0.52$). Post-hoc analyses further demonstrated that the within-domain rsFC for the tool homologous network was significantly greater than between-domain rsFC ($t_{117} = 12.4$, $p_{corrected} < 0.001$, *Cohen's d* = 1.1, Fig. 2A), suggesting the presence of an intrinsic functional network among the tool homologous regions in human neonates. The same results held when the pre-term and full-term neonates were analyzed separately (full-term neonates: $t_{105} = 11.4$, $p_{corrected} < 0.001$, *Cohen's d* = 1.1; pre-term neonates: $t_{11} = 6.3$, $p_{corrected} < 0.001$, *Cohen's d* = 1.8, Fig. S1A). No coherent face homologous network was observed in neonates, as within-face-domain rsFC was not stronger than between-domain rsFC ($t_{117} =$ -4.5, $p_{corrected} < 0.001$; i.e., in the reverse direction of the face-network presence).

Tool homologous intrinsic network structure absent in macaques. The ANOVA analysis based on the macaque dataset available in the PRIME-DE consortium revealed a significant main e ect for the di erences among the within-tool-domain, within-face-domain and between-domain rsFC ($F_{2,48} = 22.5$, $p < 0.001$, partial $\eta^2 = 0.48$). Post-hoc analyses showed that the within-tool-domain rsFC was not stronger than between-domain rsFC ($t_{24} = -3.95$, $p = 0.001$; i.e., in the reverse direction of the tool-network presence, Fig. 2A), indicating that the homologous regions derived from the tool processing ROIs in human adults did not form an intrinsic brain network structure in the macaque brain. In contrast, a face homologous network was observed using the same approach, as within-face-domain rsFC was significantly greater than between-domain rsFC ($t_{24} = 4.5$, $p_{corrected} < 0.001$, *Cohen's d* = 0.90, Fig. 2A). The presence of the face homologous network in macaques was further replicated both in a subsample of 9 macaques who were awake during scanning ($t_8 = 5.6$, $p_{corrected} = 0.001$, *Cohen's d* = 1.9) and 16 macaques who macaques

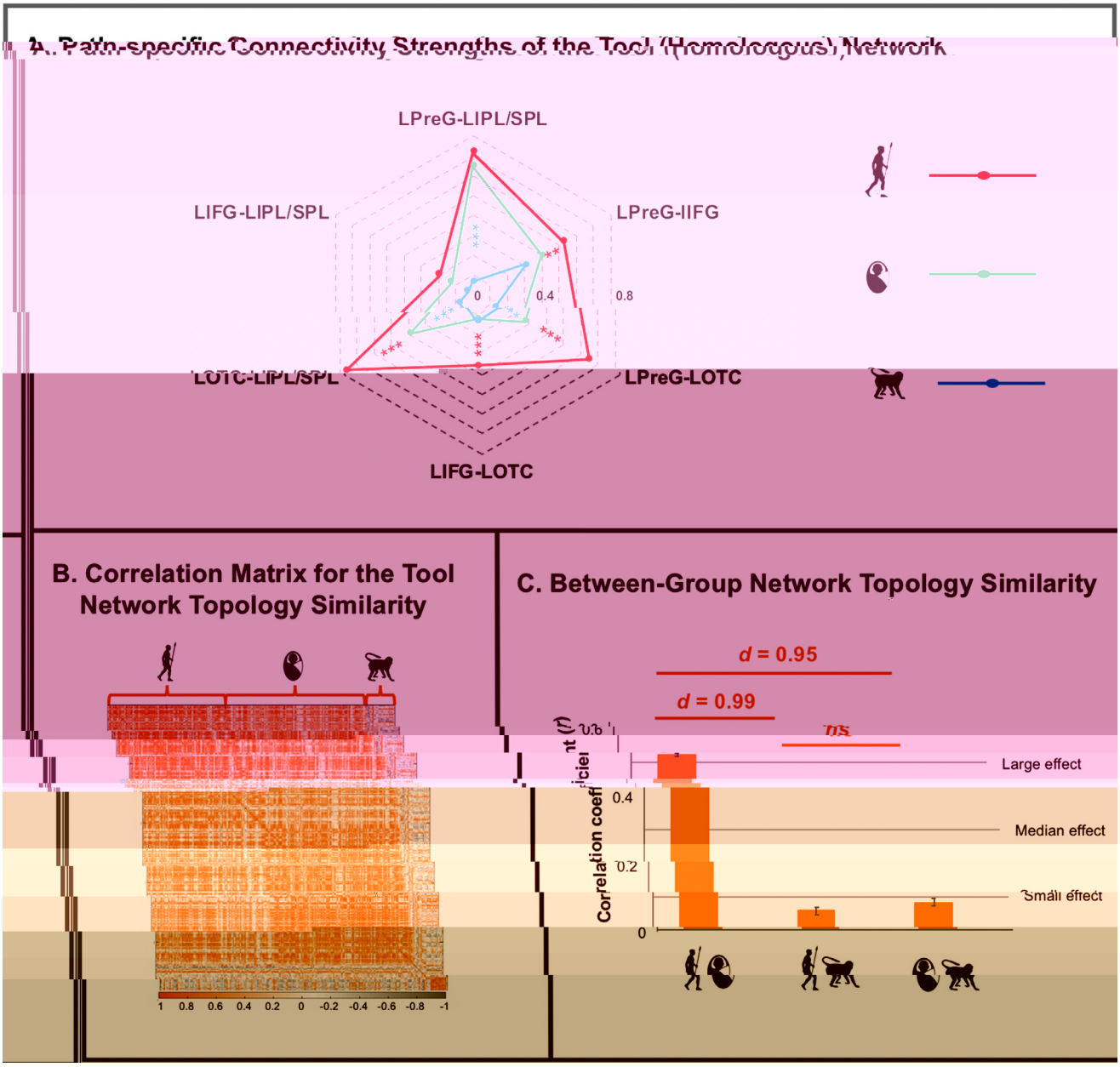

Fig. 3. High topological similarities for the tool (homologous) network between human adults and neonates, but not between humans and macaques. A. Path-specific connectivity strengths (Fisher Z scores) of the tool (homologous) network in all three groups. Significant group comparisons between human adults and human neonates are marked in ✻, whereas significant group di erences between human neonates and macaques are marked in ✻. The left premotor-left inferior/superior parietal path was species-specific, since it was the only path that was comparable between human adults and human neonates, but di erent between human neonates and macaques. * $p_{corrected} < 0.05$, ** $p_{corrected} < 0.01$, *** $p_{corrected} < 0.001$. B. The correlational matrix for the network topology similarities in all three populations for the tool processing network. C. Bar graphs show tool network topology similarities for participants belonging to di erent groups. E ect sizes (Cohen's d) are shown for comparisons in which significant di erences in between-group pattern similarities were observed (all $p_{corrected} < 0.001$). Error bars indicate standard errors.

groups. Fig. 3A visualizes the topological pattern of the tool (homologous) network for each group by showing the path-wise rsFC strengths. The stronger similarity between the human adult and human neonate groups shown in the figure was further confirmed by the topological similarity results on the tool (homologous) processing network (see Fig. 1C for the method and Fig. 3B for the cross-subject correlation matrix across all subjects). Specifically, the topological patterns of the tool (homologous) networks in human adults and neonates were significantly correlated with large e ect sizes ($r = 0.52 \pm 0.48$, one-sample $t_{11799} = 119.3$, $p_{corrected} < 0.001$, *Cohen's d* = 1.1, Fig. 3C). By contrast, the similarities between the macaque group and either human group were, although statistically significant, very low (human adults-macaques: $r = 0.054 \pm 0.49$, one-sample $t_{2499} = 5.1$, $p_{corrected} < 0.001$, *Cohen's d* = 0.10; human neonates-macaques, $r = 0.080 \pm 0.48$, one-sample $t_{2949} = 8.4$, $p_{corrected} < 0.001$, *Cohen's d* = 0.15, Fig. 3C). The ANOVA analysis on the between-group similarities among the three group pairs further revealed a significant main

t_{14748} = 46.0, $p_{corrected}$ < 0.001, *Cohen's d* = 0.95, Fig. 3C), while the latter two did not di er significantly from each other (t_{5448} = 1.8, p = 0.07).

To deal with the limited number of connections (n=6) in the tool processing network that might impact the topological similarity results, a validation analysis was conducted, in which the time series of each participant was split into 10 bins, resulting in 60 data points per subjects for the topological similarity computation. This validation analysis revealed the same result pattern as reported here (see Supplementary Materials 1.3 for details).

For the face homologous network, all between-group correlations for the face (homologous) network were significant with large or medium e ect sizes (human adults-neonates: r = 0.51 ± 0.26, one-sample t_{11799} = 234.0, $p_{corrected}$ < 0.001, *Cohen's d* = 2.2; human adults-macaques: r = 0.47 ± 0.21, one-sample t_{2499} = 116.7, $p_{corrected}$ < 0.001, *Cohen's d* = 2.3; human neonates-macaques, r = 0.43 ± 0.25, one-sample t_{2949} = 100.0, $p_{corrected}$ < 0.001, *Cohen's d* = 1.8, Fig. S5). The ANOVA analysis demonstrated significant group di erences in the between-group similarities among the three group pairs ($F_{2,17247}$ = 229.9, p < 0.001, partial η^2 = 0.03). Post-hoc analyses showed that the topological patterns for the face (homologous) network were more similar between human adults and neonates than between human adults and macaques (t_{14298} = 11.1, $p_{corrected}$ < 0.001, *Cohen's d* = 0.25), which were in turn were more similar than those between human neonates and macaques (t_{5448} = 6.6, $p_{corrected}$ < 0.001, *Cohen's d* = 0.18, Fig. S5). The network topology results mostly remained for both the tool and face processing networks when pre-term and full-term neonates and when awake and anesthetized macaques were analyzed separately (Fig. S2).

3.3. Nodal and path results: Strong contributions of premotor connectivity to the formation of the intrinsic tool homologous network in human neonates

Is the formation of the tool (homologous) network in human adults and neonates driven by any particular region(s) or functional connection(s)? This question was addressed using leave-one-node/path-out analyses (Fig. 1D). In human adults, when any single node/path was removed, the remaining network still showed stronger within- than between-domain rsFC (all *ts* > 5, all $p_{corrected}$ < 0.001, Fig. S6A), suggesting that the tool processing network was robust in human adults (see the same result patterns derived from the left-hemispheric nodes in Fig. S6B). By contrast, in human neonates, when the left premotor node was removed, the remaining tool processing nodes no longer formed an intrinsic network (t_{117} = 1.2, p = 0.24). Removal of any other node or path did not a ect the presence of the tool homologous network (i.e., within-tool-domain - between-domain rsFC > 0, all *ts* > 4, all $p_{corrected}$ < 0.001, Fig. 4A). Furthermore, the same analyses were repeated using only the left-hemispheric nodes, to ensure balanced within-tool-domain and between-domain nodal distances. All results were replicated except that the removal of the left inferior/superior parietal node or its connection with the left premotor node made the tool homologous network no longer observable (node removal results: t_{117} = 0.24, p = 0.81; path removal results: t_{117} = 1.9, p = 0.06, Fig. 4B). That is, the connection between left premotor and left inferior/superior parietal nodes (LPreG-LIPL/SPL) is particularly important for the presence of the intrinsic tool homologous network at birth in humans (see replication of the results for nodal and path contributions in subsamples of pre-term and full-term neonates in Fig. S7).

The path results were further corroborated by the direct group comparisons on the rsFC of each path, as visualized in Fig. 3A. The LPreG-LIPL/SPL connection was the most comparable between human adults and neonates, with smallest *t* value in two-sample comparisons between human adults and neonates (Table S3) and significantly lower rsFC differences when compared with most of other paths (Table S4). Meanwhile, this LPreG-LIPL/SPL connection also revealed the strongest differences between human neonates and macaques (Fig. 3A), with the largest *t* value in two-sample comparisons (Table S3) and significant group x path interaction e ects when contrasted with other paths (Table S4). In addition, while the LPreG was significantly connected to the LIPL/SPL in both human adults and neonates (*ts* > 5, $p_{corrected}$ < 0.001), this connection was not significantly above zero in the macaque brain (t_{24} = 1.54, p = 0.14), further suggesting the species-specific nature of this path.

4. Discussion

To test whether the intrinsic brain connectivity structure supporting tool processing observed in human adults is driven by individual object manipulation experience or is predisposed in humans, we compared their resting-state functional connectivity (rsFC) in this network to homologous networks in human neonates (without manipulation experience) and mature/adolescence macaques (with motor experience with objects), using face (homologous) networks as references. We found that the brain regions that are homologous to those supporting tool processing in human adults were more strongly intrinsically connected with each other than with other nodes (face homologous regions) in the human neonate brain, thereby forming an intrinsic functional network. The homologous regions in macaques did not, however, show a greater within-tool-domain rsFC when compared to the between-domain connectivity. The overall topological patterns among these regions were also highly similar between human adults and human neonates, and much less similar between humans and macaques. The left premotor region, especially its functional connection with the parietal cortex, was particularly important in the formation of the tool homologous network in human neonates.

It should first be acknowledged that the nodes evaluated in human neonate and macaque brains were transformed from regions-of-interest defined in human adult brains using advanced registration methods, including the recently developed cross-species functional alignment approach (Xu et al., 2020) and tools o ered by ANTs (Avants et al., 2009). The transformation to neonates' and other species' brains is not a trivial task, and is more than a technical challenge. Precise transformation applies if a structure is fully conservative – having the same anatomical and functional correspondence across species (and developmental stage for the case of neonate-adult comparison), which is actually exactly the question at stake here – to what extent the brain system supporting tools is conservative across species and/or "innate" in humans. The approach taken here is to use the state-of-art transformation approach for each population of interest, and the same approach for regions/networks of interest (tool cognition) and for regions that previously have shown to be relatively conservative (as control; face regions). The cross-species functional alignment approach we adopted here uses a joint-embedding technique that represents the functional organization of human and macaque brains in a high-dimensional common space. This method allows for cortical transformation between species, which had been suggested as the state-of-art transformation approach (Liu et al., 2021; Van Essen et al., 2019). The face homologous nodes in the macaque brain obtained using this transformation approach were largely consistent with those identified based on task-based fMRI studies in macaques (Hesse and Tsao, 2020; Ku et al., 2011; Landi and Freiwald, 2017; Tsao et al., 2008). The observation of the significant similarity of the face network between macaques and humans, and not the tool network derived from the same transformation approach, suggests the "human tool network" was not as conservative. Furthermore, convergence was also obtained using ROIs derived from the anatomically-defined atlas available for each population that approximated the functional ROIs, which, although less precise, circumvent the transformation processes (Supplementary Materials 1.2). These di erent types of cross-species brain mapping rely on di erent sets of assumptions, and the convergence across di erent approaches increases the confidence of the findings.

Our main observations were that the tool homologous network is present in human neonates, but not significantly identified in macaques,

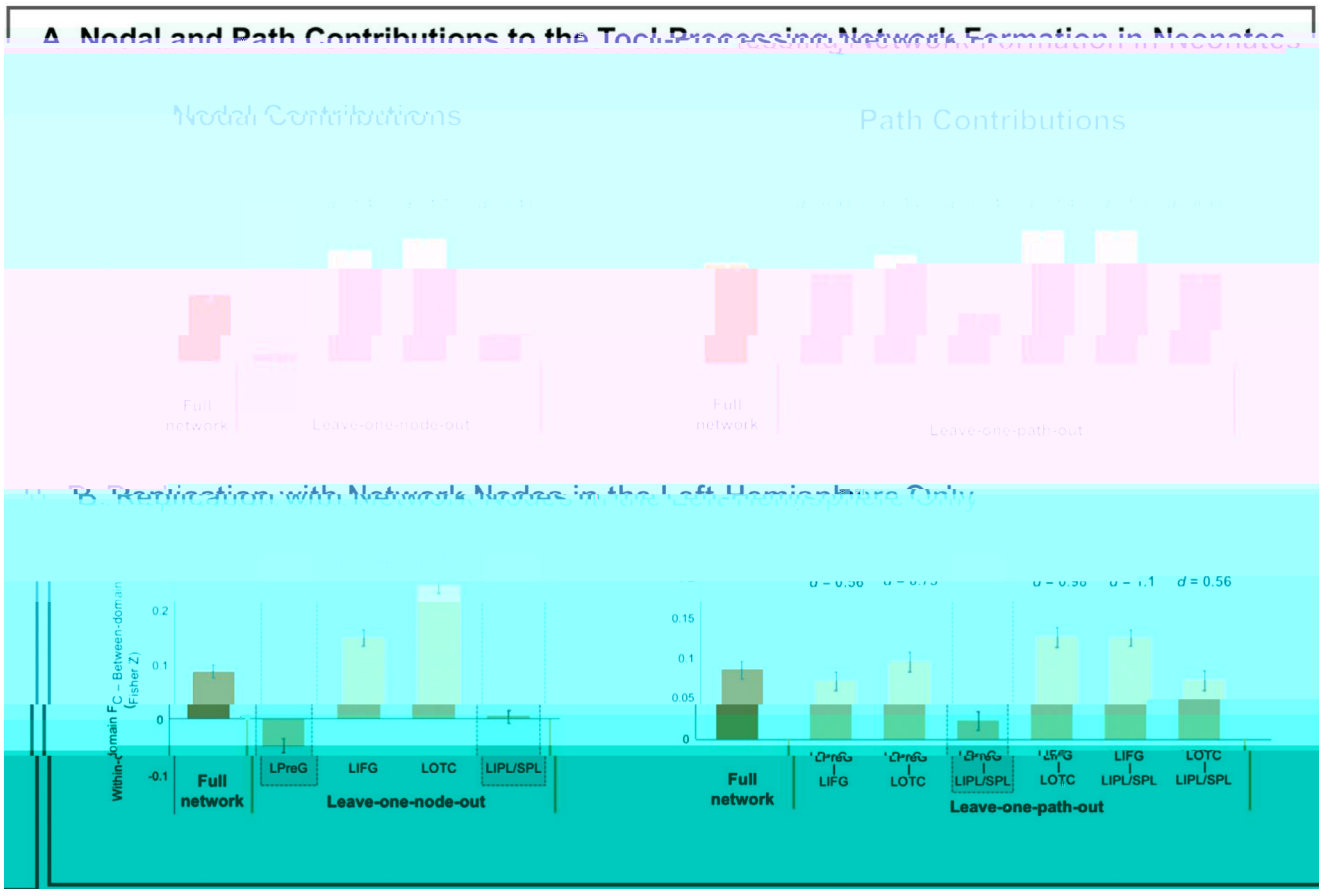

Fig. 4. Critical contributions of the premotor region and its connectivity with the parietal region to the formation of the intrinsic tool homologous network in human neonates, as revealed by leave-one-node/path-out analyses. A. Bar graphs illustrate network e ects, calculated as within-domain minus between-domain rsFC, for the full tool network and when each of the constituent nodes (left column) or path (right column) is removed. B. Bar graphs exhibit results of the leave-one-node/path out analysis derived from left-hemispheric nodes with balanced within-tool-domain and between-domain path length. E ect sizes (Cohen's d) are shown when the rsFC of the remaining tool network were still significantly higher than that of the between-domain connections (all $p_{corrected} < 0.001$). Error bars indicate corresponding standard errors. LOTC: left lateral occipitotemporal cortex; LIPL/SPL: left inferior and superior parietal lobule; LPreG: left premotor gyrus; LIFG: left inferior frontal gyrus; rsFC: resting-state functional connectivity

and that the intrinsic functional connectivity pattern of this network is more similar between human adults and human neonates than between human adults and macaques. This composite pattern suggests that the tool processing network may be (at least partly) specific to humans, and is in place early in human development. This network is not (fully) driven by simple sensorimotor experiences per se, as for human neonates, the voluntary grasping is not developed until 2–6 months old (Touwen, 1995), let alone to manipulate tools. By contrast, although there are no documented data on object interaction experiences of the macaques in the current dataset, they were mature or adolescent in age, typically with developed sensorimotor skills at least for grasping objects such as food. Worth emphasizing is that we are not claiming that this network is not associated with sensorimotor experience at all. In human adults, the tool processing network showed robust within- than between-domain rsFC after the removal of any node or path, revealing that the tool network e ect in human adults is not driven by any single node/path but rather is a composite pattern where the overall connectivity is tight to support tool use. Moreover, the functional connectivity for the tool processing network tended to be stronger for human adults than for neonates, indicating the sculpting effects of postnatal experiences. Nevertheless, the developmental changes of the tool network are not at odds with its presence in neonates, as the latter suggests that sensorimotor experiences, at least in primary forms such as grasping, are not fully necessary (in neonates) or su cient (in macaques) for this network structure to emerge at the first place.

In macaques, a brain network supporting hand grasping abilities has been identified, including AIP, F5, m12r/m46v, and TEa/m (Borra et al., 2017; Howells et al., 2020; Premereur et al., 2015). The tool homologous network discussed here partly overlaps with this grasping network (Fig. S8) and their relationship is worth specific discussion. Cognitively, tool processing in humans certainly involves grasping, but goes beyond simple grasping an object and entails an understanding of how to manipulate it in a way appropriate for functional use, based on the causal/mechanical relationship between its physical properties, use, and function (e.g., Watson and Buxbaum 2015). Neurally, various kinds of properties about tools such as shape, grasping, and manipulation knowledge, are preferentially represented by di erent brain regions in the human adult brain (e.g., parietal cluster for shape/grasping/manipulation; frontal cluster for manipulation; see e.g., Wang et al. 2018, Wu et al. 2020). Species di erences were observed in the left inferior parietal cortex, with IPL typically being activated during tool activity viewing in humans and not macaques (Kastner et al., 2017; Peeters et al., 2009), and showing significant di erences between humans and macaques in terms of anatomical (Cheng et al., 2021) and functional connectivity patterns (Xu et al., 2020). Aligning with these previous findings, we also found that the functional connectivity of the parietal cluster (with premotor cluster) was most saliently di erent be-

tween species (humans and macaques) and similar within species (human adults and neonates).

It is thus tempting to associate the observed intrinsic functional network pattern showing species di erence, the parietal-premotor connection in particular, to those cognitive components showing species di erence, i.e., the causal (mechanic) understanding (as opposed to similar components such as grasping and/or simple sensorimotor associations). The current consensus from the cognitive/behavioral studies is that whe7091 Tff7.9701 0 0 7.9701 144.4131 656.jf/F1 1 Tff7.9701 0 0 7.9701 37.911 646.344 Tmf.f6.3(ciat8 6.3761 131.10s)Tjf/F1 1 Tff7.

Washington University. The neonate data were provided by the developing Human Connectome Project, KCL-Imperial-Oxford Consortium, which is funded by the European Research Council under the European Union Seventh Framework Programme (FP/2007-2013) / ERC Grant Agreement no. [319456]. The macaque data were provided by investigative teams from Oxford (Principal Investigators: Jerome Sallet, Rogier B. Mars, Matthew F.S. Rushworth) and funded by the Wellcome Trust, Royal Society, Medical Research Council UK and the

McLaren, D.G., Kosmatka, K.J., Kastman, E.K., Bendlin, B.B., Johnson, S.C., 2010. Rhesus macaque brain morphometry: a methodological comparison of voxel-wise approaches. Methods 50, 157–165. doi:10.1016/j.ymeth.2009.10.003.

McLaren, D.G., Kosmatka, K.J., Oakes, T.R., Kroenke, C.D., Kohama, S.G., Matochik, J.A., Ingram, D.K., Johnson, S.C., 2009. A population-average MRI-based atlas collection of the rhesus macaque. NeuroImage 45, 52–59. doi:10.1016/j.neuroimage.2008.10.058.

Milham, M.P., Ai, L., Koo, B., Xu,

Brochier, T., Chen, A., Croxson, P.L., Damatac, C.G., Dehaene, S., Everling, S., Fair,

Hadj-Bouziane, F., Ben

ner, S., Klink, P.C., Kwok, S.C., Laland, K.N., Leopold, D.A., Lindenfors, P., Mars, R.B., Menon, R.S., Messinger, A., Meunier, M., Mok, K., Morrison, J.H., Nacef, J., Nagy, J., Rios, M.O., Petkov, C.I., Pinsk, M., Poirier, C., Procyk, E., Rajimehr, R., Reader, S.M., Roelfsema, P.R., Rudko, D.A., Rushworth, M.F.S., Russ, B.E., the

anatomical repre

connectome

Peeters,